J Arid Land (2023) 15(4): 393–406
https://doi.org/10.1007/s40333-023-0099-z

Science Press Springer-Verlag

# Wind dynamic environment and wind-sand erosion and deposition processes on different surfaces along the Dunhuang–Golmud railway, China

ZHANG Hongxue[1,2], ZHANG Kecun[1*], AN Zhishan[1], YU Yanping[3]

[1] Dunhuang Gobi Desert Research Station, Northwest Institute of Eco-Environment and Resources, Chinese Academy of Sciences, Lanzhou 730000, China;
[2] University of Chinese Academy of Sciences, Beijing 100049, China;
[3] Gansu Agricultural University, Lanzhou 730000, China

**Abstract:** The Dunhuang–Golmud railway passes through different deserts in arid areas, especially drifting-sand desert and sandy-gravel Gobi. The near-surface wind environment and wind-sand transport process vary due to different external factors, such as topography, vegetation, and regional climate, resulting in evident spatial differences in surface erosion and deposition. Consequently, the measures for preventing wind-sand hazards will differ. However, the mechanism and control theory of sand damage remain poorly understood. In this study, we used meteorological observation, three-dimensional (3D) laser scanning, and grain-size analysis to compare and evaluate the spatial distribution of wind conditions, sand erosion and deposition patterns, and grain composition in the drifting-sand desert and sandy-gravel Gobi along the Dunhuang–Golmud railway in China. Results show that the annual mean wind speed, the frequency of sand-driving wind, and the drift potential of sandy-gravel Gobi are higher than those of drifting-sand desert, indicating a greater wind strength in the sandy-gravel Gobi, which exhibits spatial heterogeneity in wind conditions. The major sediment components in sandy-gravel Gobi are very fine sand, fine sand, and medium sand, and that in drifting-sand desert are very fine sand and fine sand. We found that the sediment in the sandy-gravel Gobi is coarser than that in the drifting-sand desert based on mean grain size and sediment component. The spatial distributions of sand erosion and deposition in the sandy-gravel Gobi and drifting-sand desert are consistent, with sand deposition mainly on the west side of the railway and sand erosion on the east side of the railway. The area of sand deposition in the drifting-sand desert accounts for 75.83% of the total area, with a mean deposition thickness of 0.032 m; while the area of sand deposition in the sandy-gravel Gobi accounts for 65.31% of the total area, with a mean deposition thickness of 0.028 m, indicating greater deposition amounts in the drifting-sand desert due to the presence of more fine sediment components. However, the sand deposition is more concentrated with a greater thickness on the embankment and track in the sandy-gravel Gobi and is dispersed with a uniform thickness in the drifting-sand desert. The sand deposition on the track of the sandy-gravel Gobi mainly comes from the east side of the railway. The results of this study are helpful in developing the preventive measures and determining appropriate selection and layout measures for sand control.

**Keywords:** surface erosion and deposition; wind environment; three-dimensional (3D) laser scanner; drift potential; grain-size characteristic; Dunhuang–Golmud railway

**Citation:** ZHANG Hongxue, ZHANG Kecun, AN Zhishan, YU Yanping. 2023. Wind dynamic environment and wind-sand erosion and deposition processes on different surfaces along the Dunhuang–Golmud railway, China. Journal of Arid Land, 15(4): 393–406. https://doi.org/10.1007/s40333-023-0099-z

*Corresponding author: ZHANG Kecun (E-mail: kecunzh@lzb.ac.cn)
Received 2022-12-09; revised 2023-03-06; accepted 2023-03-21

## 1 Introduction

Railway sand damage in desert areas has aroused widespread concern (Zhang et al., 2007; Zhang et al., 2010, 2012a; Xiao et al., 2014; Cheng et al., 2015; Lavasani et al., 2016; Mehdipour et al., 2019; Horvat et al., 2021), which involves railway safety issues. The Dunhuang–Golmud railway passes through the desert area in Northwest China, connecting Dunhuang City in Gansu Province and Golmud City in Qinghai Province. It was put into operation in December 2019, remarkably shortening the distance between the two destinations and promoting local economic and social development. However, deserts along the railway have a bare sandy surface, sparse vegetation, scarce rainfall, and frequent windblown sand activity. The railway is particularly susceptible to wind-blow sand damage, especically from the Mingsha Mountains to the Shashangou area (Yao, 2015; Yu, 2021). Aeolian sand covers the tracks and blocks culverts, threatening the safe operation of railway. A sand-blocking fence with a length of several hundred meters and a height of 1.5 m has been installed on the west side of the railway to mitigate sand damage in some areas. However, previous studies have shown that although sand control measures can intercept most sand grains, a large amount of sand particles will inevitably still deposit on the railway (Zhang et al., 2010, 2012a; Shi et al., 2020). In addition, sand control measures deployed in some areas without reference to actual wind conditions and sand damage mechanisms have often been ineffective, leading to a waste of resources.

Some scholars have observed that spatial heterogeneity occurs in the wind environment within some area caused by differences in land use, topography, vegetation cover, and sand source (Zhang et al., 2012b; Cheng et al., 2015; Zhang et al., 2018; Liu et al., 2019). This wind environment influences the activities of windblown sand (Kurosaki and Mikami, 2003). The intensities of windblown sand activities affect the release and transport of dust as well as the erosion and deposition processes of sand (Wang et al., 2005, 2006). The differences in ground surface types along the railway also affect the wind environment, resulting in differences in windblown sand activities and erosion and deposition patterns. Therefore, the same sand control measures may be ineffective on different surface types. Previous studies on wind dynamic environments mainly focused on single underlying surface, lacking comparative studies on different underlying surface types (Zu et al., 2008; Cheng et al., 2015; Zhang et al., 2015). Therefore, studying the wind environment and erosion and deposition patterns of different desert types is essential for developing effective measures for controlling sand damage along the railway.

In previous studies, wind tunnel experiments (Dong et al., 2003; Zhang et al., 2007; Duan et al., 2013; Raffaele et al., 2016) and numerical simulations (Li and Martz, 1994; Andreotti, 2004; Wakes et al., 2010; Kang, 2012; Baniamerian et al., 2015; Zhou et al., 2016; Cheng et al., 2017) were used to study the wind speed, the transport of windblown sand, erosion and deposition pattern on the desert surface (Iversen et al., 1990; Farimani et al., 2011; Ferreira and Fino, 2012; Lopes et al., 2013), and the railway-protection systems (Alhajraf et al., 2004; Lavasani et al., 2016; Tominaga et al., 2018; Mehdipour et al., 2019). However, wind tunnel experiments and numerical simulations mainly reveal and predict the sand erosion and deposition processes. The actual amount and spatial distribution of erosion and deposition in field environment are rarely studied. As high-precision instruments, three-dimensional (3D) laser scanners can directly obtain the spatial point cloud information and construct the complex and irregular 3D visualization model, which can accurately monitor the erosion and deposition characteristics of sandy material in the field. They have been successfully applied in studying aeolian geomorphology, such as the topography changes of star dunes (An et al., 2018, 2022; Herzog et al., 2022), making them a promising tool for studying sand damage in desert areas along the railway.

The sandy-gravel Gobi and drifting-sand desert are the areas most remarkably affected by sand damage along the railway. In this study, we used meteorology observation, 3D laser scanning, and grain size analysis to compare and evaluate the dynamic wind environment and erosion and deposition characteristics in the sandy-gravel Gobi and drifting-sand desert, clarifying the mechanism of sand damage to the railway. This study can provide a scientific basis for the

relevant researchers to select and implement effective sand control measures in areas with different underlying surface types.

## 2 Study area

The Dunhuang–Golmud railway, covering a total length of 616.79 km (Yu, 2020), is located in the arid desert area of China, with widely distributed dunes and Gobi. The railway extends from north to south (Fig. 1), with the north side connecting the sandy-gravel Gobi and the Mingsha Mountains and the south side connecting the piedmont alluvial-diluvial plain of Altun Mountains (Yao, 2015). The northwest is characterized by the Kumtag Desert, with mobile, semi-fixed, and fixed dunes that provide rich material that may exacerbate railway damage. The climate of the study area is a typical hyper arid continental climate, characterized by average annual precipitation of less than 100 mm, frequent strong winds, sparse vegetation, and vulnerability to windblown sand damage. Field investigation has shown that the railway sand damage is mainly distributed between Mingsha Mountains and Shashangou area based on the sediment deposition on the railway track (Yu, 2020), where the annual number of intense windy days over 150 d and belongs to the plain alluvial area with a flat terrain. The strong winds provide sufficient energy to entrain considerable amounts of windblown sand, causing sand damage to the railway track.

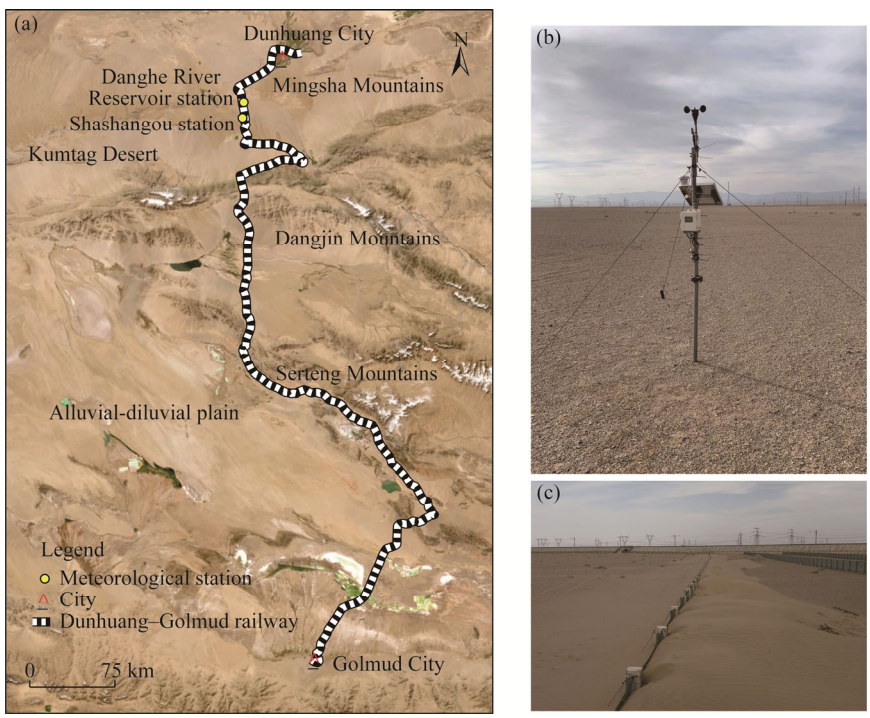


**Fig. 1** Overview of the Dunhuang–Golmud railway (a) and the photos of the sandy-gravel Gobi (b) and drifting-sand desert (c)

The total length of the railway affected by sand damage from Mingsha Mountains to Shashangou area is about 16.5 km, including the sandy-gravel Gobi and drifting-sand desert. In order to study the aeolian environments and sand transport characteristics, we set up two meteorological stations in the railway sand damage area. The meteorological data for the sandy-gravel Gobi were collected from the Danghe River Reservoir station (94°20′31″E, 39°52′19″N; Fig. 1b), where the terrain is flat and broad. The observation data for the drifting-sand desert were acquired from the Shashangou station (94°20′41″E, 39°47′35″N; Fig. 1c), where the surface has widespread shifting sand with the thickness of the sand layer ranging from 5 to 100 m.

## 3 Data and methods

Meteorological observation data were obtained from self-recording anemometers placed at a height of 2 m above the ground, measuring 16 compass azimuths at intervals of 10 min. The observation period was from June 2019 to May 2020. Mean wind speed, the frequency of sand-driving wind, and sand drift potential (DP) were calculated in the sandy-gravel Gobi and drifting-sand desert. Sand DP was calculated using the following equation (Fryberger, 1979):

$$\mathrm{DP} = V^2 \left(V - V_t\right) t, \tag{1}$$

where DP is drift potential and the unit is vector unit (VU); $V$ is the measured wind speed (m/s); $V_t$ is the threshold speed for sand movement ($V_t$=5.00 m/s); and $t$ is the duration of wind at speed $V$, expressed as a percentage of the total time (%). Resultant drift potential (RDP; VU) represents the net DP (magnitude and direction) based on a summation of the DP values in each compass azimuth. We calculated the RDP and the resultant drift direction (RDD; °) according to the law of vectors composition. An index of the directional variability of the wind is the ratio of the RDP to the DP, herein known as RDP/DP.

The 3D laser scanner (RIEGL VZ2000, RIEGL Laser Measurement Systems GmbH, Vienna, Austria) can provide measurements between 580 and 2050 m, and was used to acquire topographic data. The scanning geometry of the scanner is up to 360.0° horizontally and up to 100.0° vertically, and its single measurement error is 0.05 m per 100.00 m. Topographic data included field operations and indoor work. During field operations, point clouds were acquired from three scan positions on 8 May 2019 and from three scan positions on 22 May 2020. These positions were mainly distributed around the railway embankment to obtain high coverage. Multi-station and multiple periods scanning only provide the local coordinate system; however, postprocessing requires a unified coordinate system. Therefore, cylindrical reflector targets were placed around the scan positions as the control point before scanning. In order to ensure that the scanned data were within an identical coordinate system, we used Global Positioning System Real-time kinematic (GPS RTK) to obtain their position coordinates.

For indoor work, we used the Automatic Registration and Multi-station Adjustment tool in RiSCAN Pro software to splice the multistation data, then converted the local coordinate system to the same coordinate system using the cylindrical reflector coordinates, ensuring that the error was within 6 mm, and finally utilized the terrain filtering tool to eliminate noisy points and generate a text file. We converted the text file into points using ArcGIS software, generating a triangulated irregular network (TIN) from the points. The TIN was transformed into a raster data model, and area and volume were calculated by using the Raster Calculator and Surface Volume tool, respectively. The amount of wind erosion and deposition was obtained by using the Raster Subtract tool.

We selected sampling sites in the sandy-gravel Gobi and sand-driving desert, including the railway track, the east slope, east slope foot, west slope, and west slope foot of the railway. Then, we set 10 sampling sites and collected 3 sediment samples at each site, resulting in a total of 30 sampling samples. We used a laser grain-size instrument (Mastersizer 2000, Malvern Instruments UK Ltd., Malvern, England) to measure the grain size of each sample three times and computed the average value. Mean grain size, sorting coefficient, and skewness were calculated by using the formulas of Folk and Ward (1957).

## 4 Results

### 4.1 Wind characteristics

The annual mean wind speed and the frequency of sand-driving wind on the surfaces of the sandy-gravel Gobi were 2.61 m/s and 8.97%, respectively, while those on the surfaces of the drifting-sand desert were 2.43 m/s and 6.99%, respectively. In the sandy-gravel Gobi, the annual sand DP was 65.56 VU, and RDP and RDD were 27.33 VU and 191.68°, respectively (Fig. 2). In the drifting-sand desert, the annual sand DP was 45.91 VU, and the RDP and RDD were 18.51 VU and 174.65°, respectively (Fig. 2b). During the observation period, three distinct wind

directions were observed in the two regions, i.e., northwest (including west-northwest (WNW), northwest (NW), and north-northwest (NNW)), northeast (including east-northeast (ENE) and northeast (NE)), and east winds.

Considering the north-south direction of the railway, sand-driving winds from west and east will have a greater impact on sand damage. The easterly winds in the sandy-gravel Gobi accounted for 56.28%, with the wind speed of 5.00–6.00 m/s accounting for 25.56% and the wind speed of 6.00–7.00 m/s accounting for 13.63%. In addition, in the sandy-gravel Gobi, the westerly winds accounted for 36.49%, with the wind speed of 5.00–6.00 m/s accounting for 17.17% and the wind speed of 6.00–7.00 m/s accounting for 8.97%. The easterly winds in the drifting-sand desert was 39.96%, with the wind speed of 5.00–6.00 m/s accounting for 18.50% and the wind speed of 6.00–7.00 m/s accounting for 9.98%. Furthermore, in the drifting-sand desert, the westerly winds were 50.27%, with the wind speed of 5.00–6.00 m/s accounting for 24.59% and the wind speed of 6.00–7.00 m/s accounting for 12.79% (Fig. 3).

From the perspective of time series, the monthly variations of the frequency of sand-driving wind and mean wind speed in the sandy-gravel Gobi and drifting-sand desert presented a consistent trend (Fig. 4). The monthly mean wind speed and the frequency of sand-driving wind from April to August were noticeably higher, with a remarkable decline from September to the following March. In addition, the monthly mean wind speed and the frequency of sand-driving wind in the sandy-gravel Gobi were slightly higher than that in the drifting-sand desert.

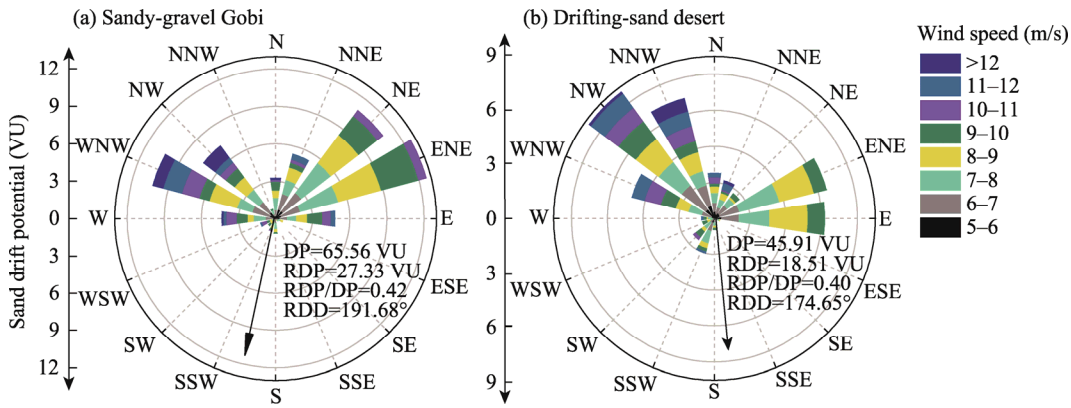


**Fig. 2** Rose of sand drift potential (DP) in the sandy-gravel Gobi (a) and drifting-sand desert (b). RDP and RDD represent resultant drift potential and resultant drift direction, respectively. N, north; NNE, north-northeast; NE, northeast; ENE, east-northeast; E, east; ESE, east-southeast; SE, southeast; SSE, south-southeast; S, south; SSW, south-southwest; SW, southwest; WSW, west-southwest; W, west; WNW, west-northwest; NW, northwest; NNW, north-northwest.

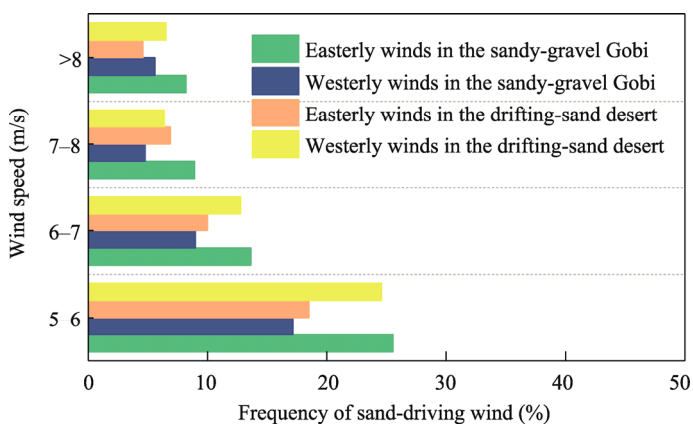


**Fig. 3** Frequency of sand-driving wind of easterly and westerly winds in the sandy-gravel Gobi and drifting-sand desert

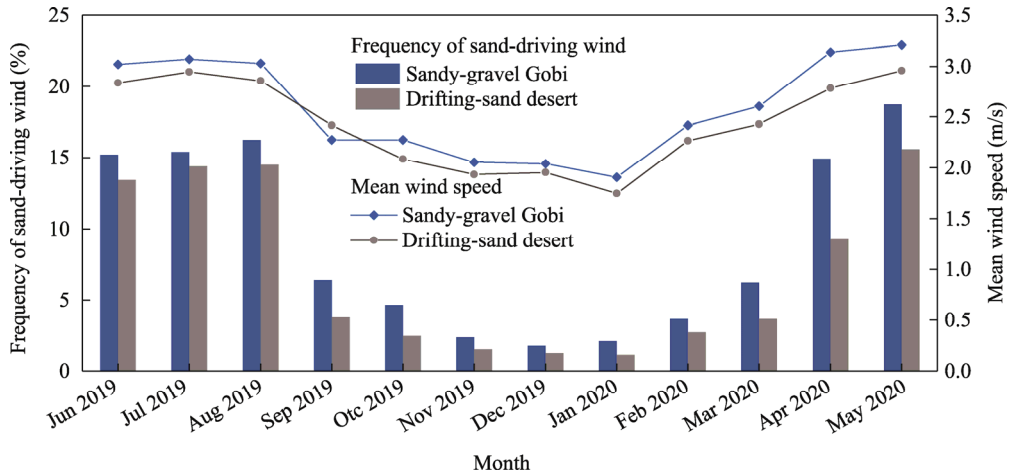


**Fig. 4** Monthly variation of the frequency of sand-driving wind and mean wind speed in the sandy-gravel Gobi and drifting-sand desert

### 4.2 Sand erosion and deposition on the surfaces of the sandy-gravel Gobi and drifting-sand desert

During the observation period (May 2019–May 2020), the surface deposition sand in the sandy-gravel Gobi accounted for 65.31% of the total area (52,511.117 $m^2$), with a deposition volume of 976.107 $m^3$, a maximum deposition thickness of 0.276 m, and a mean deposition thickness of 0.028 m. Surface eroded by wind occupied 34.69% of the total area, and the wind erosion volume amounted to 190.234 $m^3$. The maximum and average erosion depth was 0.053 and 0.010 m, respectively (Fig. 5). Surface deposition was remarkably greater than erosion, and sand deposition was mainly concentrated near the fence and two sides of the embankment. The deposition thickness between 0.000 and 0.020 m accounted for the largest proportion of the total area, accounting for 31.13%, followed by a deposition thickness of 0.020–0.040 m, which accounted for 16.54% (Fig. 5e). These results indicated that most measurements of deposition thickness were below 0.040 m.

We selected the P1–P1′, P2–P2′, and P3–P3′ sections on the west side of the railway, embankment, and the east side of the railway, respectively, to analyse the erosion and deposition amounts in each region. Many large and dense sand-deposition zones around P1–P1′ section gradually became sparse near the railway (Fig. 5a). In Figure 5b, the maximum thickness of deposition sand on the west side of the fence was 0.157 m, and the maximum thickness on the east side of the fence was 0.165 m. The sand-deposition zone stretching for 100 m to the east gradually thinned, indicating that the sand-blocking effect of the fence was pronounced. The P2–P2′ section spans the railway embankment (Fig. 5a), which depicted a large amount of sand centrally deposited on the west side of the embankment with a large thickness, and the maximum thickness was 0.213 m (Fig. 5c). Sand deposition was observed on the railway track, with a maximum deposition thickness of 0.075 m, indicating that the fence has not entirely prevented sand damage. On the east side of the embankment, the deposition sand distributed dispersedly with a smaller deposition thickness (0.104 m and below). According to the P3–P3′ section (Fig. 5d), we found the erosion and deposition were coexisting. However, erosion was dominant and the surface erosion depth was mainly at the centimeter level, with a maximum erosion depth being 0.042 m.

The statistical results showed that the area of the sand deposition in the drifting-sand desert accounted for 75.83% of the total area (63,438.892 $m^2$), with a deposition volume of 1522.549 $m^3$, a maximum deposition thickness of 0.199 m, and a mean deposition thickness of 0.032 m. Surface wind erosion area accounted for 24.17% of the total area, with a wind erosion amount of 150.806 $m^3$, and the maximum and mean erosion depths of 0.048 m and 0.010 m, respectively (Fig. 6). The

surface deposition volume was 10 times the erosion amount. Deposition was predominantly focused on two sides of the embankment and fence. The area with deposition thickness below 0.020 m was the largest, accounting for 31.42% of the total area, followed by the deposition thickness of 0.020–0.040 m (21.72%) and 0.040–0.060 m (11.92%; Fig. 6e).

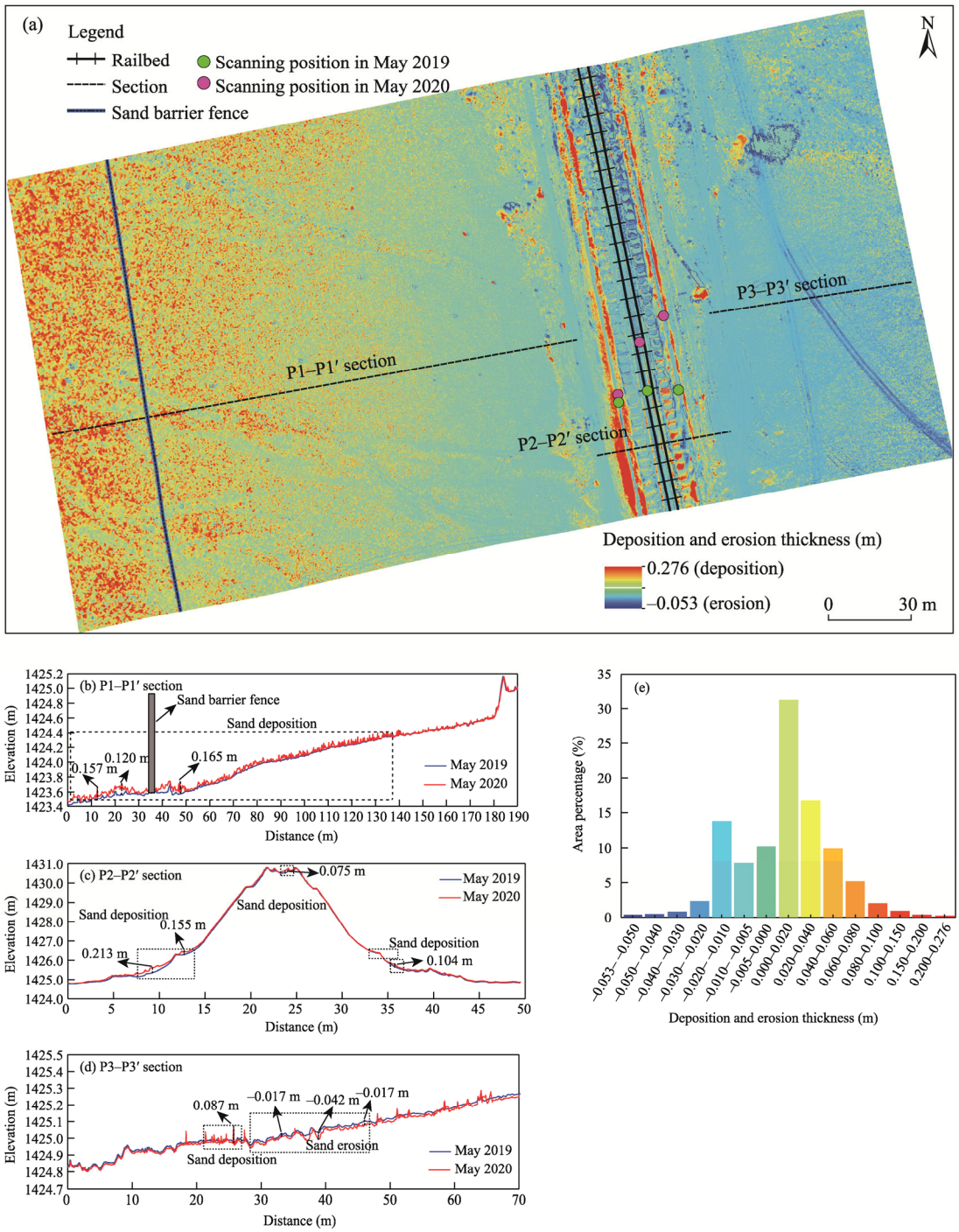


**Fig. 5** (a), erosion and deposition on the surfaces of the sandy-gravel Gobi; (b, c, and d), elevation changes along the P1–P1′ P2–P2′ and P3–P3′ sections, respectively; (e), the area percentage of different deposition and erosion thicknesses on the surfaces of the sandy-gravel Gobi. The positive values of deposition and erosion thickness indicate sand deposition, and the negative values of deposition and erosion thickness represent erosion.

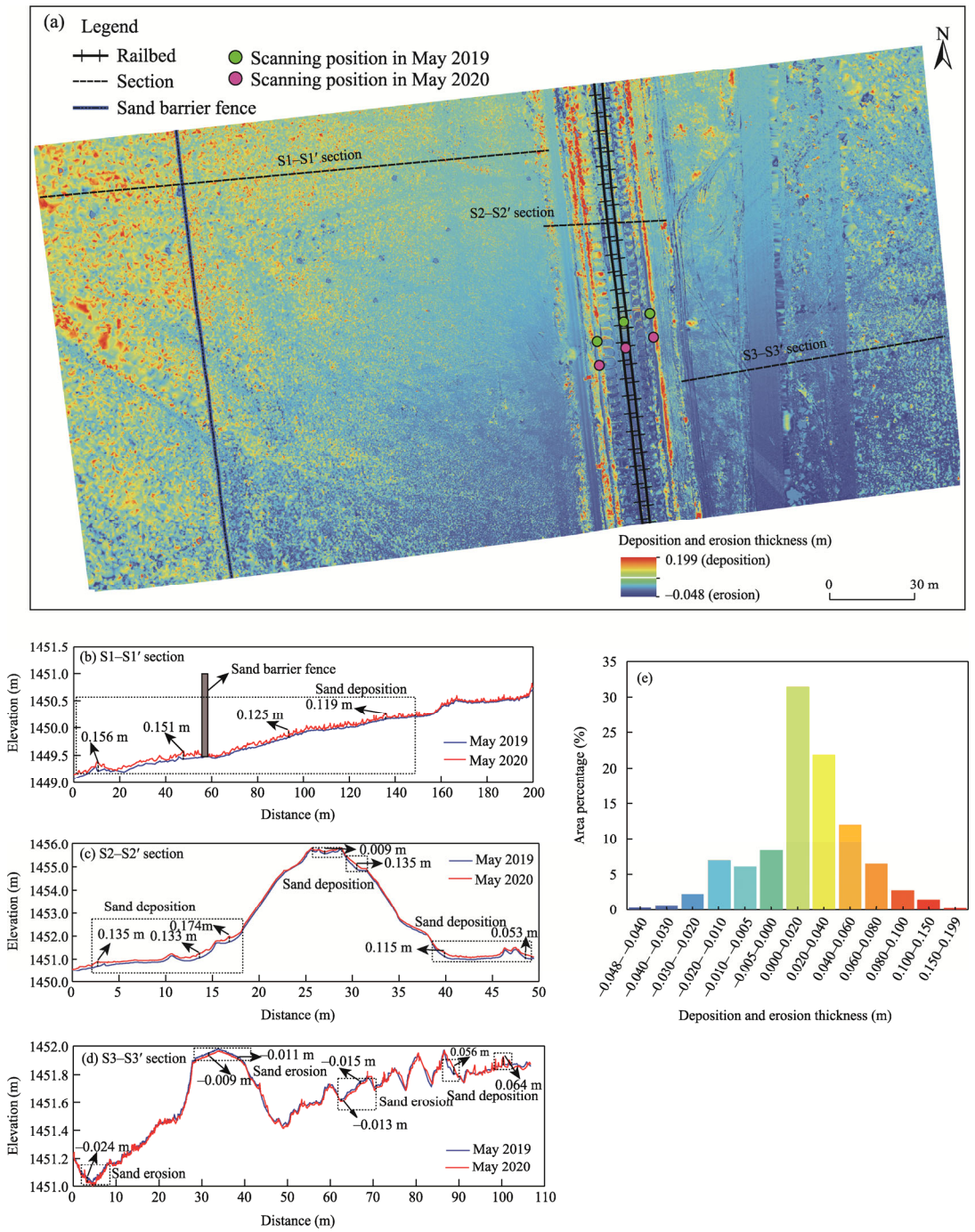


**Fig. 6** (a), erosion and deposition on the surfaces of the drifting-sand desert; (b, c, and d), elevation changes along the S1–S1′, S2–S2′, and S3–S3′ sections, respectively; (e), the area percentage of different deposition and erosion thicknesses on the surfaces of the drifting-sand desert. The positive values of deposition and erosion thickness indicate sand deposition, and the negative values of deposition and erosion thickness represent erosion.

In the S1–S1′ section, a large amount of sand deposited near the fence, with maximum deposition thickness of 0.156 and 0.125 m on the west and east sides of the fence, respectively; and sand-deposition zone stretching for 140 m to the east gradually thinned. Large amounts of sand deposited on both sides of the embankment. In the S2–S2′ section (Fig. 6c), the variation in sand deposition thickness was relatively slight and uniform, with a maximum thickness of 0.174

m on the west side. The sand deposition was thicker on the east side of the embankment with a maximum thickness of 0.135 m, and sand deposition with a thickness of 0.009 m appeared on the railway tracks. In the S3–S3′ section (Fig. 6d), erosion and deposition coexisted, but erosion was predominant, with an erosion depth ranging from 0.010 to 0.030 m and the maximum erosion depth being 0.024 m.

The spatial distributions of sand erosion and deposition on the surfaces of the sandy-gravel Gobi and drifting-sand desert were consistent. The surface was dominated by deposition and supplemented by erosion, sand mainly deposited on the both sides of the embankment and fence, and wind erosion mainly occurred on the east side of the railway. The area proportion and the mean thickness of the sand deposition on the surface of the drifting-sand desert were larger than those on the surface of the sandy-gravel Gobi. However, the sand deposition on the embankment and track of the sandy-gravel Gobi was more concentrated and had greater thickness, whereas it was dispersed with a uniform thickness on the surface of the drifting-sand desert.

### 4.3 Grain size distribution of sediments in the sandy-gravel Gobi and drifting-sand desert

Figure 7 shows the grain size distribution of sediments in the sandy-gravel Gobi and drifting-sand desert. In the sandy-gravel Gobi, grain size distribution of sediments was mostly unimodal, except for the east slope and east slope foot of the railway (Fig. 7a). The peak values of the grain size distribution curves tended to increase from the railway track to the two sides of the slope foot. The positions of peak values gradually shifted toward larger grain size values, indicating that the particles became coarser from the railway track to the east and west sides. The mean grain size of sediments on the railway track was the smallest (155.60 μm), which gradually increased to the east (336.63 μm) and west (201.98 μm) sides (Table 1). The sediments on the railway track had the highest content of fine sand (60.27%) and very fine sand (26.50%) without coarse sand, very coarse sand, and gravel, and the total content of coarse sand, very coarse sand, and gravel on the east side of the railway was up to 27.36%. The above data show that the sediments on the railway track are the finest.

The sorting coefficient of aeolian sediments is an objective indicator used to measure the intensity of the blown sand activity, and the larger the sorting coefficient, the poorer the sorting. In the sandy-gravel Gobi, the sediments on the railway track had the smallest sorting coefficient (0.62), followed by the sediments on the west slope of the railway (0.69), and the sediments on the east slope foot of the railway (1.41) had the largest sorting coefficient, indicating that sorting of the east slope foot of the railway was the worst.

In the drifting-sand desert, the grain size distribution of one sediment sample on the railway track and three samples on the west slope foot of the railway were bimodal, and the rest sediments samples on other sites were unimodal (Fig. 7b). The peak values of the grain size composition curves of all sampling sites were extremely close. The mean grain size of sediments on the railway track was the largest (170.10 μm), which gradually decreased to the east (135.49 μm) and west (146.46 μm) sides (Table 1). The total content of fine sand and very fine sand in the drifting-sand desert was 70.00%–85.00%. The sediments on the west slope of the railway had the highest fine sand content (50.39%), while the sediments on the railway track had the most extensive very fine sand content (37.14%). The sediments on the railway track and the east slope of the railway contained a small amount of coarse sand, very coarse sand, and gravel. The sediments on the railway track were the coarsest, whereas they were finer on the east and west sides of the railway. In the drifting-sand desert, the sorting coefficient of sediments on the west slope foot of the railway and the railway track was larger, and that on the east slope foot of the railway and the west slope of the railway was smaller. A negative skewness value (–0.17) was observed on the sediments on the railway track and the west slope foot of the railway, and the sediments at the remaining sampling sites were nearly symmetrically distributed.

The sediments near the railway in the sandy-gravel Gobi were mainly composed of very fine sand (14.00%–26.00%), fine sand (36.00%–60.00%), and medium sand (9.00%–29.00%). The major components in the drifting-sand desert were very fine sand (30.00%–37.00%) and fine sand

(34.00%–50.00%), with finer components in the drifting-sand desert and coarser components in the sandy-gravel Gobi. The mean grain size gradually increased from the railway track to the east and west sides of the railway in the sandy-gravel Gobi, but an opposite trend was observed in the drifting-sand desert.

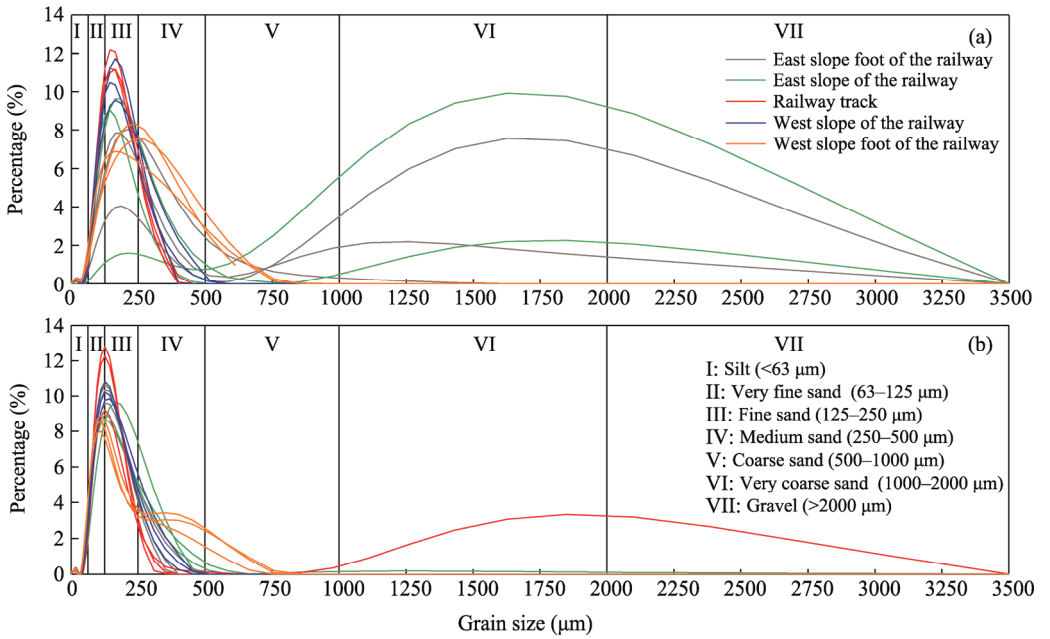


**Fig. 7** Grain size distribution of sediments in the sandy-gravel Gobi (a) and drifting-sand desert (b). Each color has three grain size distribution curves, representing three samples from the same sampling site.

**Table 1** Grain size composition and characteristic in the sandy-gravel Gobi and drifting-sand desert

| Desert type | Sample site | Grain size composition | | | | | | | Grain size characteristic | | |
|---|---|---|---|---|---|---|---|---|---|---|---|
| | | Silt (%) | Very fine sand (%) | Fine sand (%) | Medium sand (%) | Coarse sand (%) | Very coarse sand (%) | Gravel (%) | *Mz* (μm) | *σ* | *SK* |
| Sandy-gravel Gobi | ESF | 5.17 | 14.23 | 36.67 | 16.56 | 6.13 | 14.29 | 6.94 | 336.63 | 1.41 | 0.09 |
| | ES | 3.51 | 16.38 | 36.05 | 10.94 | 5.66 | 17.64 | 9.83 | 333.36 | 1.07 | 0.11 |
| | RT | 3.76 | 26.50 | 60.27 | 9.48 | 0.00 | 0.00 | 0.00 | 155.60 | 0.62 | 0.07 |
| | WS | 4.49 | 24.24 | 57.04 | 14.13 | 0.10 | 0.00 | 0.00 | 165.06 | 0.69 | 0.06 |
| | WSF | 6.88 | 17.36 | 41.19 | 29.09 | 5.48 | 0.00 | 0.00 | 201.98 | 0.98 | 0.13 |
| Drifting-sand desert | ESF | 8.87 | 34.88 | 49.42 | 6.70 | 0.13 | 0.00 | 0.00 | 135.49 | 0.75 | 0.10 |
| | ES | 7.89 | 30.01 | 47.75 | 12.94 | 1.08 | 0.25 | 0.08 | 150.43 | 0.81 | 0.03 |
| | RT | 4.94 | 37.14 | 48.31 | 2.66 | 0.24 | 3.81 | 2.89 | 170.10 | 0.98 | –0.17 |
| | WS | 6.62 | 34.36 | 50.39 | 8.53 | 0.10 | 0.00 | 0.00 | 141.79 | 0.71 | 0.03 |
| | WSF | 10.68 | 35.83 | 34.50 | 12.30 | 6.70 | 0.00 | 0.00 | 146.46 | 1.00 | –0.17 |

Note: *Mz*, mean grain size; *σ*, sorting coefficient; *SK*, skewness. ESF, ES, RT, WS, and WSF represent the east slope foot of the railway, the east slope of the railway, the railway track, the west slope of the railway, and the west slope foot of the railway, respectively.

## 5 Discussion

### 5.1 Comparison of wind environment

The data obtained from the meteorological station showed that the sandy-gravel Gobi and drifting-sand desert belong to the low-wind environment (<200 VU) with the consistent intrayear

trend variation. However, the wind speed, the frequency of sand-driving wind, and sand DP in the sandy-gravel Gobi were remarkably higher than that in the drifting-sand desert, indicating the spatial heterogeneity of wind conditions. Several studies have made similar findings. For example, the wind conditions from north to south in the Kumtagh, Tengger, Badain Jaran, and Taklamakan deserts are different (Zhang et al., 2012; Zhang et al., 2015; Liu et al., 2019); and the spatial patterns of different dune types and shapes have a reasonable correlation with wind regimes (Hereher, 2018; Hu et al., 2021). Zhang et al. (2018) believed that differences in aeolian environments between the desert and sandy lands are caused by differences in geography, climate, and vegetation types. However, meteorological stations in the sandy-gravel Gobi and drifting-sand desert are only 13.9 km apart, and no differences are observed in climate and vegetation type between the two regions. Therefore, we concluded that the local terrains caused a slight difference in the wind environment of the two regions, such as the extensive Gobi surface and the drifting-sand surface that is undulated by sand dunes.

### 5.2 Surface erosion and deposition characteristics

The west side of the railway experienced prominent deposition and the east side of the railway suffered noticeable erosion in the sandy-gravel Gobi and drifting-sand desert. Some studies have found that sand generally accumulates on the windward slope of obstacles, with wind erosion occurring on the leeward side (Smyth et al., 2019; Cai et al., 2021; Herzog et al., 2022). However, the two regions suffer from westerly and easterly winds without a single prevailing wind direction, so the windward and leeward slopes cannot explain erosion and deposition. The fence on the west side of the railway acts an obstacle to the wind-sand flow, changing the airflow characteristics and forming different airflow regions (Zhang et al., 2012a), as well as reducing the wind speed and resulting in sand deposition near the fence (Xiao et al., 2014; Cheng et al., 2017; Wang et al., 2018). A substantial source of sand was intercepted by fence in advance, so the deposition of sand near the embankment was reduced. The eastern side of the railway was unobstructed, resulting in high wind speeds and sand flows, which carried away sandy material and caused surface erosion.

The surface deposition area in the sandy-gravel Gobi accounted for 65.31%, with a mean deposition thickness of 0.028 m. In comparison, the surface deposition area in the drifting-sand desert occupied 75.83%, with a mean deposition thickness of 0.032 m. The sedimentary effect in the drifting-sand desert was more evident than that in the sandy-gravel Gobi. Wang et al. (2021) found that the horizontal mass flux of sand transport in sand desert is remarkably higher than that in gravel Gobi. The more abundant sand sources may be the reason of the sedimentary effect in the drifting-sand desert. The total content of silt and very fine sand in the drifting-sand desert was 40.00%–50.00%, but it was only 20.00%–30.00% in the sandy-gravel Gobi. Silt and very fine sand are fine components in the sediments of the drifting-sand desert and are more conducive to transport and deposition on the surface (Shen et al., 2020). Surface erosion in the sandy-gravel Gobi seems more obvious, with an erosion area of 34.69% and a maximum erosion depth of 0.053 m, compared with the surface erosion in the drifting-sand desert, with an erosion area of 24.17% and a maximum erosion depth of 0.048 m, which is probably related to the wind environment.

### 5.3 Spatial variation of grain size

The mean grain size represents the sediment distribution trend, reflecting the average kinetic energy of the transport medium. The grain size distribution of sediments is essential to analyze and determine the wind erosion processes at the eroded surface (Pye, 1987; Warren, 2013; Zhang et al., 2016). In the sandy-gravel Gobi, the sediments on the easterly side of the railway (mean grain size=336.63 μm) were coarser than those on the westerly side of the railway (mean grain size=201.98 μm), and the sorting on the easterly side was poorer (sorting coefficient=1.41) than that on the westerly side (sorting coefficient=0.98). According to statistics, sand-driving wind from the easterly direction makes up 56.28% with a wind speed above 7.00 m/s of 17.10%, and wind from the westerly direction accounts for 36.49% with a wind speed above 7.00 m/s of 10.34%. This finding illustrated that the easterly winds were more frequent and stronger than

westerly winds in the sandy-gravel Gobi. The height of the railway embankment in the study area is 5 m, which is a huge obstacle for easterly or westerly winds. A large number of fine grains were carried away by more frequent and stronger easterly winds from the east side of the railway, resulting in relatively coarser sediment remaining on the east side. The fine components mainly deposited on the railway track from the east side of the railway, as confirmed by the following data: the content of very fine sand and fine sand was higher on the railway track (26.50% and 60.27%, respectively) but lower on the east side of the railway (14.23% and 36.67%, respectively). Therefore, sand-control measures deployed only on the west side of the railway in the sandy-gravel Gobi are unreasonable, and the east side also needs sand-control measures due to the strong winds.

Some studies (Zhang et al., 2007; Shen et al., 2020) suggested that with the increase of near-surface wind speed, the separation effect of wind on surface sediments becomes increasingly remarkable, leading to better sorting of sediments. Based on grain size and wind data from east to west side of the railway in the sandy-gravel Gobi, we found that strong winds on the east side of the railway lead to poorer sorting of sediments, because the region became wind eroded regions with the fine component being carried away, whereas sediments with better sorting appear in deposition regions due to most particles of similar size were trapped. The east side of the railway with frequent and stronger wind belongs to the source area of sand transport, with poorer sorting and coarser sediment, whereas the sediments on the railway track, as deposition region, have better sorting and finer sand material. In the drifting-sand desert, the mean grain size and sorting coefficient do not have a clear pattern due to the slight difference in the percentage of easterly (39.96%) and westerly (50.27%) winds. The above phenomenon suggests that the analysis of the relationship between grain size and wind conditions may require the differentiation of sand transport source areas and deposition areas, which needs further in-depth study.

## 6 Conclusions

The results show that the annual mean wind speed, the frequency of sand-driving wind, and sand DP were 2.61 m/s, 8.97%, and 65.56 VU in the sandy-gravel Gobi, respectively; and they were 2.43 m/s, 6.99%, and 45.91 VU in the drifting-sand desert, respectively. The wind strength in the sandy-gravel Gobi was stronger than that in the drifting-sand desert, which exhibited the spatial heterogeneity of wind conditions. In the sandy-gravel Gobi, the sediments near the railway were mainly composed of very fine sand (14.00%–26.00%), fine sand (36.00%–60.00%), and medium sand (9.00%–29.00%), whereas the major sediments in the drifting-sand desert were very fine sand (30.00%–37.00%) and fine sand (34.00–50.00%). We found that the sediments of sandy-gravel Gobi were coarser than that of drifting-sand desert based on mean grain size and sediment component. The mean grain size gradually increased from the railway track to the east and west sides of the railway in the sandy-gravel Gobi, but an opposite trend was observed in the drifting-sand desert. In accordance with 3D laser scanning data, the sand mainly deposited on the west side of the railway, and wind erosion mainly occurred on the east side of the railway. The area percentage and average thickness of deposition sand in the drifting-sand desert (75.83% and 0.032 m, respectively) were more extensive than those in the sandy-gravel Gobi (65.31% and 0.028 m, respectively), which may be due to the presence of more fine sediments in the drifting-sand desert. However, deposition sand was more concentrated with a greater deposition thickness on the embankment and track in the sandy-gravel Gobi, whereas it was dispersed with a uniform thickness in the drifting-sand desert. On the basis of the distribution characteristics of sediment components and wind conditions, sand deposition on the railway track of the sandy-gravel Gobi mainly came from the east side of the railway.

## Acknowledgements

This research was supported by the National Natural Science Foundation of China (42171083, 41871016) and the Natural Science Foundation of Gansu Province, China (22JR5RA066).

## References


Alhajraf S. 2004. Computational fluid dynamic modeling of drifting particles at porous fences. Environmental Modelling & Software, 19(2): 163–170.

An Z S, Zhang K C, Tan L H, et al. 2018. Dune dynamics in the southern edge of Dunhuang Oasis and implications for the oasis protection. Journal of Mountain Science, 15(10): 2172–2181.

An Z S, Zhang K C, Tan L H, et al. 2022. Morphologic changes of simple star dunes during the growth process in Dunhuang, China. Journal of Mountain Science, 19(4): 1095–1106.

Andreotti B. 2004. A two-species model of aeolian sand transport. Journal of Fluid Mechanics, 510: 47–70.

Baniamerian Z, Mehdipour R, Kargar F. 2015. A numerical investigation on aero-dynamic coefficients of solar troughs considering terrain effects and vortex shedding. International Journal of Engineering, 28(6): 940–948.

Cai D X, Li S Y, Gao X, et al. 2021. Wind tunnel simulation of the aeolian erosion on the leeward side of barchan dunes and its implications for the spatial distribution patterns of barchan dunes. CATENA, 207: 105583, doi: 10.1016/j.catena.2021.105583.

Cheng J J, Jiang F Q, Xue C X, et al. 2015. Characteristics of the disastrous wind-sand environment along railways in the Gobi area of Xinjiang, China. Atmospheric Environment, 102: 344–354.

Cheng J J, Xin G W, Zhi L Y, et al. 2017. Unloading characteristics of sand-drift in wind-shallow areas along railway and the effect of sand removal by force of wind. Scientific Reports, 7(1): 41462, doi: 10.1038/srep41462.

Dong Z B, Liu X P, Wang H T, et al. 2003. Aeolian sand transport: a wind tunnel model. Sedimentary Geology, 161(1–2): 71–83.

Duan S Z, Cheng N, Xie L. 2013. A new statistical model for threshold friction velocity of sand particle motion. CATENA, 104: 32–38.

Farimani A B, Ferreira A D, Sousa A C M. 2011. Computational modeling of the wind erosion on a sinusoidal pile using a moving boundary method. Geomorphology, 130(3–4): 299–311.

Ferreira A D, Fino M R M. 2012. A wind tunnel study of wind erosion and profile reshaping of transverse sand piles in tandem. Geomorphology, 139–140: 230–241.

Folk R L, Ward W C. 1957. Brazos River bar: a study in the significance of grain size parameters. Journal of Sedimentary Research, 27(1): 3–26.

Fryberger S G. 1979. A Study of Global Sand Seas for Dune Forms and Wind Regime. Washington DC: U.S. Geological Survey Press.

Hereher M E. 2018. Geomorphology and drift potential of major aeolian sand deposits in Egypt. Geomorphology, 304: 113–120.

Herzog M, Anders K, Höfle B, et al. 2022. Capturing complex star dune dynamics-Repeated highly accurate surveys combining multitemporal 3D topographic measurements and local wind data. Earth Surface Processes and Landforms, 47(11): 2726–2739.

Horvat M, Bruno L, Khris S. 2021. CWE study of wind flow around railways: Effects of embankment and track system on sand sedimentation. Journal of Wind Engineering and Industrial Aerodynamics, 208: 104476, doi: 10.1016/j.jweia.2020.104476.

Hu Z H, Gao X, Lei J Q, et al. 2021. Geomorphology of Aeolian Dunes in the Western Sahara Desert. Geomorphology, 392: 107916, doi: 10.1016/j.geomorph.2021.107916.

Iversen J D, Wang W P, Rasmussen K R, et al. 1990. The effect of a roughness element on local saltation transport. Journal of Wind Engineering and Industrial Aerodynamics, 36(2): 845–854.

Kang L Q. 2012. Discrete particle model of aeolian sand transport: Comparison of 2D and 2.5D simulations. Geomorphology, 139–140: 536–544.

Kurosaki Y, Mikami M. 2003. Recent frequent dust events and their relation to surface wind in East Asia. Geophysical Research Letters, 30(14): 1736, doi: 10.1029/2003GL017261, 2003.

Lavasani A M, Razi P, Mehdipour R. 2016. Numerical solution of fence performance for reduction of sand deposition on railway tracks. International Journal of Engineering, 29: 1014–1021.

Li L, Martz L W. 1994. System of numeric models for sand particle transport by wind. Journal of Geophysical Research, 99(D6): 12999–13012.

Liu Z Y, Dong Z C, Zhang Z C, et al. 2019. Spatial and temporal variation of the near-surface wind regimes in the Taklimakan Desert, Northwest China. Theoretical and Applied Climatology, 138(1–2): 433–447.

Lopes A M G, Oliveira L A, Ferreira A D, et al. 2013. Numerical simulation of sand dune erosion. Environmental Fluid Mechanics, 13 (2): 145–168.

Mehipour R, Baniamerian Z. 2019. A new approach in reducing sand deposition on railway tracks to improve transportation. Aeolian Research, 41: 100537, doi: 10.1016/j.aeolia.2019.07.003.

Pye K. 1987. Aeolian Dust and Dust Deposits. London: Academic Press, 108–115.

Raffaele L, Bruno L, Pellerey F, et al. 2016. Windblown sand saltation: a statistical approach to fluid threshold shear velocity. Aeolian Research, 23: 79–91.

Shen Y P, Zhang C L, Wang R D, et al. 2020. Spatial heterogeneity of surface sediment grain size and aeolian activity in the gobi desert region of northwest China. CATENA, 188: 104469, doi: 10.1016/j.catena.2020.104469.

Shi L, Wang D Y, Li K C. 2020. Windblown sand characteristics and hazard control measures for the Lanzhou-Wulumuqi high-speed railway. Natural Hazards, 104: 353–374.

Smyth T A G, Hesp P A, Walker I J, et al. 2019. Topographic change and numerically modelled near surface wind flow in a bowl blowout. Earth Surface Processes and Landforms, 44(10): 1988–1999.

Tominaga Y, Okaze T, Mochida A. 2018. Wind tunnel experiment and CFD analysis of sand erosion/deposition due to wind around an obstacle. Journal of Wind Engineering and Industrial Aerodynamics, 182: 262–271.

Wakes S J, Maegli T, Dickinson K J, et al. 2010. Numerical modelling of wind flow over a complex topography. Environmental Modelling & Software, 25(2): 237–247.

Wang R D, Li Q, Zhang C L, et al. 2021. Comparison of dust emission ability of sand desert, gravel desert (Gobi), and farmland in northern China. CATENA, 201: 105215, doi: 10.1016/j.catena.2021.105215.

Wang T, Qu J J, Ling Y Q, et al. 2018. Shelter effect efficacy of sand fences: A comparison of systems in a wind tunnel. Aeolian Research, 30: 32–40.

Wang X M, Dong Z B, Yan P, et al. 2005. Surface sample collection and dust source analysis in northwestern China. CATENA, 59(1): 35–53.

Wang X M, Zhou Z J, Dong Z B. 2006. Control of dust emissions by geomorphic conditions, wind environments and land use in northern China: An examination based on dust storm frequency from 1960 to 2003. Geomorphology, 81(3–4): 292–308.

Warren A. 2013. Dunes: dynamics, morphology, history. New Jersey USA: Wiley-Blackwell Press.

Xiao J H, Yao Z Y, Qu J J. 2014. Influence of Golmud-Lhasa section of Qinghai-Tibet Railway on blown sand transport. Chinese Geographical Science, 25(1): 39–50.

Yao H L. 2015. Wind-sand environmental characteristics and integrated protection system of wind-sand hazards in the high dune area of Dunhuang-Geermu railway. Desert of China, 35(3): 555–564. (in Chinese)

Yu Y P. 2021. Study on formation mechanism and control of blown-sand disaster along the Dunhuang-Golmud Railway. PhD Dissertation. Lanzhou: Northwest Institute of Eco-Environment and Resources, Chinese Academy of Sciences, 23–24. (in Chinese)

Zhang C, Zou X Y, Pan X H, et al. 2007. Near-surface airflow field and aerodynamic characteristics of the railway-protection system in the Shapotou region and their significance. Journal of Arid Environments, 71(2): 169–187.

Zhang C L, Shen Y P, Li Q, et al. 2018. Sediment grain-size characteristics and relevant correlations to the aeolian environment in China's eastern desert region. Science of the Total Environment, 627(15): 586–599.

Zhang K C, Qu J J, Liao K T, et al. 2010. Damage by wind-blown sand and its control along Qinghai-Tibet Railway in China. Aeolian Research, 1(3–4): 143–146.

Zhang K C, Qu J J, Han Q, et al. 2012a. Wind tunnel simulation of windblown sand along China's Qinghai–Tibet Railway. Land Degradation & Development, 25(3): 244–250.

Zhang K C, Qu J J, An Z S. 2012b. Characteristics of wind-blown sand and near-surface wind regime in the Tengger Desert, China. Aeolian Research, 6: 83–88.

Zhang K C, An Z S, Cai D W, et al. 2016. Key role of desert-oasis transitional area in avoiding oasis land degradation from aeolian desertification in Dunhuang, Northwest China. Land Degradation & Development, 28(1): 142–150.

Zhang Z C, Dong Z B, Li C X. 2015. Wind regime and sand transport in China's Badain Jaran Desert. Aeolian Research, 17: 1–13.

Zhou X S, Zhang Y, Wang Y, et al. 2016. 3D numerical simulation of the evolutionary process of aeolian downsized crescent-shaped dunes. Aeolian Research, 21: 45–52.

Zu R P, Xue X, Qiang M R, et al. 2008. Characteristics of near-surface wind regimes in the Taklimakan Desert, China. Geomorphology, 96(1): 39–47.